Single-Spin Relaxation in a Synthetic Spin-Orbit Field

F. Borjans, D.M. Zajac, T.M. Hazard, and J.R. Petta*
Department of Physics, Princeton University, Princeton, New Jersey 08544, USA

(Received 2 November 2018; revised manuscript received 24 March 2019; published 19 April 2019)

Strong magnetic field gradients can produce a synthetic spin-orbit interaction that allows high-fidelity electrical control of single electron spins. We investigate how a field gradient impacts the spin relaxation time T_1 by measuring T_1 as a function of the magnetic field B in silicon. The interplay of charge noise, magnetic field gradients, phonons, and conduction-band valleys leads to a maximum relaxation time of 160 ms at low fields, a strong spin-valley relaxation hotspot at intermediate fields, and a B^4 scaling at high fields. T_1 is found to decrease with increasing lattice temperature as well as with added electrical noise. In comparison, samples without micromagnets have a significantly greater T_1.

DOI: 10.1103/PhysRevApplied.11.044063

I. INTRODUCTION

The Zeeman-split spin states of a single electron spin in a large magnetic field can naturally be used to define a qubit [1,2]. For spins trapped in semiconductor quantum dots, single-qubit rotations can be achieved through electron spin resonance [3,4]. Spin rotations can also be electrically driven in the presence of an intrinsic spin-orbit field [5–7] or a synthetic spin-orbit field generated by a micromagnet [8,9]. With use of nearest-neighbor exchange coupling, as first demonstrated in GaAs devices [10], two-qubit operations were recently implemented in silicon with high fidelity [11–13].

Silicon has become a favored material for spin-based quantum computing due to seconds-long spin relaxation times T_1 [14,15] and the ability to extend spin coherence times T_2 through isotopic enrichment [4,16–20]. By use of electric dipole spin resonance in a field gradient, single-spin rotations with fidelities greater than 99.9% have been obtained [9]. However, the added control enabled by the micromagnet can limit T_2 [9] and may reduce T_1 [12,13]. It is therefore necessary to understand how magnetic field gradients impact T_1.

Through more than a decade of theoretical and experimental work in GaAs [2,21–30], it is well known that spin relaxation is governed by a combination of electron-phonon coupling together with hyperfine and spin-orbit interactions. The theory for GaAs predicts a B^5 dependence of T^{-1} at high fields, where spin-orbit coupling dominates, and a B^3 dependence at low fields, where the hyperfine interaction dominates. The B^5 dependence was confirmed in early experiments [28,29], and only recently was the low-field B^3 dependence observed [30].

In contrast, the theoretical background in Si/SiGe is much-less-well developed. Part of the complication stems from the small energy scale associated with the valley states in Si/SiGe quantum dots, typically $20-300\ \mu$eV. The valley physics is further complicated by the fact that a range of valley splittings can be observed in a single device [31] and in some cases the valley splitting can be gate voltage tuned [15]. There are relatively few experimental measurements of single-spin relaxation in Si-based metal-oxide-semiconductor (MOS) devices [15,32,33] and Si/SiGe [34,35]. In addition to phonon-mediated relaxation [36], the presence of valley states can lead to spin relaxation "hotspots" when the valley splitting E_V is comparable to the Zeeman energy E_Z [15,37]. However, the addition of a micromagnet to spin-qubit devices may result in new relaxation pathways, as electrical noise will lead to uncontrolled motion of the electron in the field gradient and will give rise to a randomly fluctuating magnetic field.

In this paper, we examine the impact of a synthetic spin-orbit field on single-spin relaxation in Si. To better isolate the effect of a micromagnet, we compare T_1 for devices fabricated with and without Co micromagnets. We find significantly faster spin relaxation in the micromagnet device over a 6-T range of the magnetic field. Consistent with measurements on Si-based MOS devices, we observe spin relaxation hotspots at intermediate fields [15]. However, there is an unexpected saturation of T_1 at low magnetic fields in the micromagnet device [32] and an overall weak power-law scaling at high fields for both devices. T_1 decreases with increasing temperature and added electrical noise, suggestive of a spin relaxation mechanism involving charge-noise-induced motion in a spin-orbit field.

*petta@princeton.edu

II. MEASUREMENT

We measure T_1 as a function of the external magnetic field B_{ext} on two devices (see Fig. 1) fabricated from the same Si/SiGe wafer used in previous experiments [31,38]. Electrons in the Si quantum well are laterally confined with use of an overlapping aluminum-gate architecture [31]. Device 1 consists of a double quantum dot (DQD) and an additional 250-nm-thick Co micromagnet [12]. Device 2 is a linear array of nine dots with no micromagnet [39]. Single-spin qubits are defined in the upper half of each device, and charge detection is performed by measuring the current through a charge detector located in the lower half of the device (I_S for device 1, and I_{S_1} or I_{S_2} for device 2). All measurements are performed in a dilution refrigerator, and B_{ext} is applied along the [1 1 0] crystallographic direction.

We begin by presenting measurements obtained from device 1. The charge-stability diagram is shown in Fig. 1(c) and is obtained by differentiating the charge-sensor current I_S as a function of the gate voltages V_L and V_R. The DQD is tuned to the one-electron regime, where spin relaxation measurements can be performed in the left dot near the (0,0)-(1,0) charge transition or in the right dot near the (0,0)-(0,1) charge transition, far detuned from the (1,0)-(0,1) transition, allowing the treatment as isolated quantum dots. Here (NL, NR) refer to the number of electrons in the left dot and the right dot, respectively. Before we measure T_1, the micromagnet is magnetized by ramping the external field up to 6 T.

The spin T_1 of a single electron is measured with a three-step Elzerman pulse sequence, as illustrated by points A, B, and C in Fig. 1(c) [40]. The device is first emptied of electrons at point A, after which a random spin electron is loaded into the left dot by abrupt pulsing to point B. After a time τ, the spin state is read out through spin-to-charge conversion at point C. The pulse sequence is completed by pulsing back to point A. Similarly, the right-dot spin T_1 is measured near the (0,0)-(0,1) charge transition (points A', B', and C').

Repeating the pulse sequence for various wait times τ allows measurement of the spin-up probability $P_\uparrow(\tau)$. We extract T_1 by fitting $P_\uparrow(\tau)$ to the form $P_\uparrow(\tau) = a\exp(-\tau/T_1) + b$ [41], where a and b depend on the initialization and read-out fidelities of the spin-up state [14,30,35]. The read-out visibility prohibits measurements below 0.15 T. We therefore measure between 0.15 and 6 T (the maximum field of our vector magnet).

III. RESULTS AND DISCUSSION

Spin relaxation data from device 1 are shown in Fig. 2, where we plot T_1^{-1} versus B_{ext} for the left and right dots. We observe three magnetic field regimes, where T_1 shows qualitatively different behavior. For $B_{\text{ext}} < 300$ mT, T_1 saturates around 65 ms for the left dot and 160 ms for the right dot. In the intermediate-field regime, where 0.3 T $< B_{\text{ext}} <$ 1 T, we observe a dramatic peak in T_1^{-1} for both dots, where $T_1^{-1} > 1$ kHz. This is consistent with a spin relaxation hotspot due to spin-valley mixing when E_Z is comparable to E_V [15]. Above $B_{\text{ext}} \sim 1$ T, the relaxation rates follow a power law with $T_1^{-1} \propto B_{\text{ext}}^{4.0(3.8)}$ for the left (right) dot. In general, a high-field power-law dependence is expected, but with a larger exponent (B_{ext}^5 in GaAs and B_{ext}^7 in Si/SiGe) [21,37].

To better isolate the effect of the micromagnet on T_1, we characterize device 2, which is fabricated on the same heterostructure as device 1 but has no micromagnet. The accumulation gates for device 2 are designed to create a linear chain of nine tunnel-coupled quantum dots, whose charge states can be read out with three proximal quantum-dot charge sensors. Details on the fabrication of device

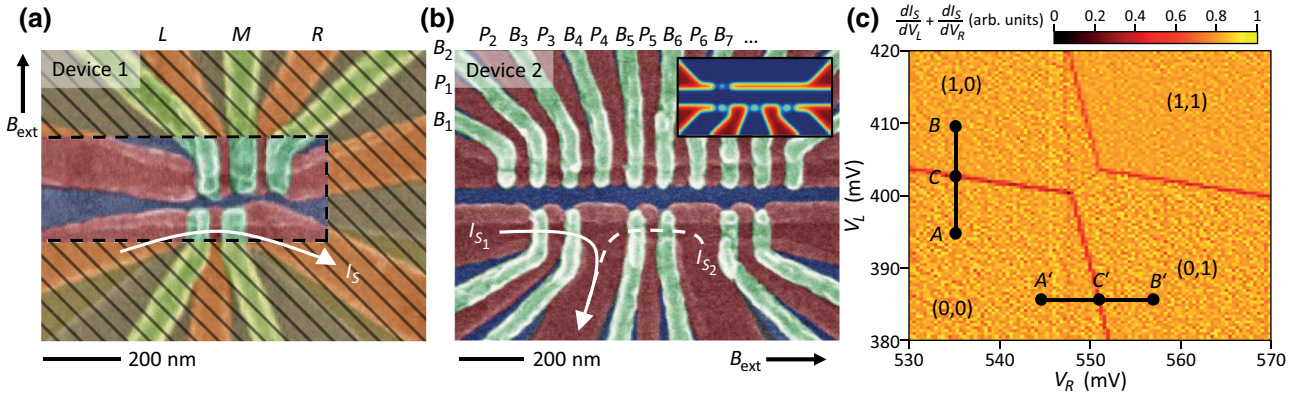

FIG. 1. False-color scanning electron micrographs of the devices used for the T_1 measurements. (a) DQD device containing an additional Co micromagnet (hashed region) for electric dipole spin resonance. (b) Nine-dot device without a micromagnet. (c) Charge stability diagram acquired with the DQD. The pulse sequence used to measure T_1 is overlaid on the data. The T_1 measurement starts with an empty DQD at position A, loads a random spin and waits for a time τ at point B, and determines the final spin state at point C using spin-to-charge conversion.

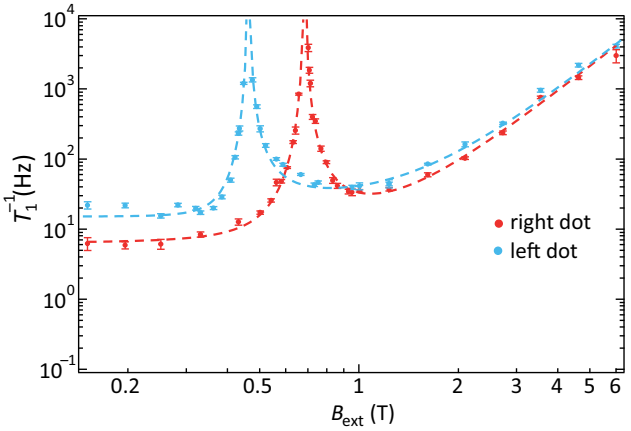

FIG. 2. T_1^{-1} from the left and right dots in device 1 (with a Co micromagnet). T_1 saturates at low field in both dots, yielding $T_1 = 65$ ms (160 ms). Spin relaxation hotspots are observed at intermediate fields of $B_{ext} = 0.47$ T (0.68 T) for the left (right) dot. For $B_{ext} > 1$ T, $T_1^{-1} \propto B_{ext}^{4.0(3.8)}$ for the left (right) dot.

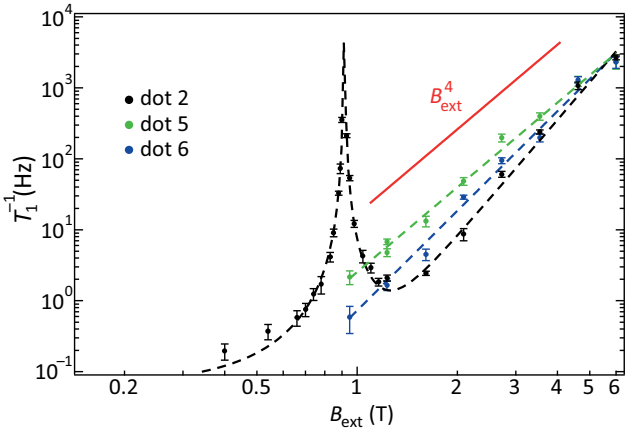

FIG. 3. T_1^{-1} for dots 2, 5, and 6 of device 2 (no micromagnet). No saturation in T_1 is observed down to $B_{ext} = 0.4$ T, where $T_1 = 5$ s. Dot 2 exhibits a relaxation hotspot at $B_{ext} = 0.915$ T. At high fields, $T_1^{-1} \propto B_{ext}^{5.5}$ (dot 2), $T_1^{-1} \propto B_{ext}^{4.0}$ (dot 5), and $T_1^{-1} \propto B_{ext}^{4.7}$ (dot 6).

2 and data showing single-electron occupancy through charge detection are presented in Ref. [39]. Since our devices operate in accumulation mode, device 2 can be used to measure T_1 of a single electron confined in a dot formed beneath any of the nine plunger gates [labeled P_1, P_2, etc. in Fig. 1(b)]. To illustrate the mode of operation of device 2, the inset in Fig. 1(b) shows a COMSOL MULTIPHYSICS simulation of the electron density in the Si quantum well. Here a single quantum dot is defined under plunger gate P_2. With the exception of barrier gates B_2 and B_3, the remaining plunger and barrier gates of the array are positively biased to accumulate a channel of electrons that connects to a two-dimensional Fermi sea, permitting full measurement of dot 2. T_1 measurements can be performed on other dots in the array by simply reconfiguring the gate voltages, where the low cross capacitance between neighboring gates guarantees local control over the confinement potentials and comparability between the measurements [31].

Figure 3 shows T_1^{-1} versus B_{ext} for dots 2, 5, and 6 in device 2. Overall, the relaxation rates are slower in device 2, especially at low magnetic fields. Specifically, T_1 approaches 5 s at $B_{ext} = 400$ mT, almost 2 orders of magnitude greater than for device 1 at the same B_{ext}. Here the T_1 measurements are restricted to $B_{ext} \geq 400$ mT, as T_1 exceeds several seconds and the measurements become very time-consuming at low field. As with device 1, we observe a peak in T_1^{-1} at intermediate fields in dot 2. However, no relaxation hotspot is observed in dots 5 and 6, presumably due to a valley splitting that lies below the minimum Zeeman energy $E_Z = 110$ μeV for these data sets. For $B_{ext} > 2$ T, $T_1^{-1} \propto B_{ext}^p$, with p exhibiting dot-to-dot variations and generally falling in the range $4 < p < 6$. Additional data for device 2 are given in Ref. [41].

We fit the data from both devices to a three-component function:

$$T_1^{-1}(\omega_Z) = T_{1,sat}^{-1} + (c_J\omega_Z + c_{ph}\omega_Z^5)F_{SV}(\omega_Z) + c_p\omega_Z^p. \quad (1)$$

The first term, $T_{1,sat}^{-1}$, is an empirical magnetic-field-independent relaxation rate that captures the low-field saturation observed in experiment, and $\omega_Z = E_Z/\hbar$ is the Larmor precession frequency. The second term in Eq. (1) accounts for spin-valley relaxation at the hotspot and includes a Johnson-noise term $c_J\omega_Z$ and a phonon-noise term $c_{ph}\omega_Z^5$, where c_J and c_{ph} are scaling prefactors. These noise terms were included in previous analyses of spin relaxation rates in Si-based MOS devices [15,33]. The behavior near the hotspot is captured by

$$F_{SV}(\omega_Z) = 1 - \left[1 + \frac{\Delta^2}{(E_V - \hbar\omega_Z)^2}\right]^{-1/2}, \quad (2)$$

which is parameterized by E_V and the spin-valley mixing energy Δ [37]. The final term in Eq. (1) reproduces the high-field behavior with power-law exponent p and scaling prefactor c_p as free parameters to account for the observed variations between dots and devices.

Fits to the data from device 1 are shown by the dashed lines in Fig. 2. To account for the additional field contribution from the micromagnet, we set $\omega_Z = g\mu_B B_{tot}/\hbar$, with $B_{tot} = B_{ext} + B_m$ and $B_m = 140$ mT, where $g = 2$ is the g factor in silicon and μ_B is the Bohr magneton. While the external field and the micromagnet field will generally add to the total field as $\vec{B}_{tot} = \vec{B}_{ext} + \vec{B}_m$, on the basis of the symmetry of the design [12] and the centered alignment of the quantum dots with respect to the gap of the micromagnet, we expect $\vec{B}_{ext} \parallel \vec{B}_m$ and therefore the simplified addition of magnitudes. From the low-field behavior we extract

$T_{1,\mathrm{sat}}^{-1} = 15.3$ Hz (6.3 Hz) for the left (right) dot. The spin-valley contribution to the total relaxation rate agrees well with the data in the vicinity of the hotspots and allows us to extract valley splittings of $E_V = 70$ μeV (95 μeV) when taking into account the field added by the micromagnet. These valley splittings are consistent with values obtained through magnetospectroscopy and dispersive read-out on similar devices [31,42]. At high fields we find power-law exponents $p = 4.0 \pm 0.1$ (3.8 ± 0.1). Here the strong spin-valley hotspot contribution to the spin relaxation rate limits the precision of p.

The data from device 2 shown in Fig. 3 are also well fit by Eq. (1). We extract a valley splitting $E_V = 106$ μeV in dot 2, but ignore the spin-valley contribution in dots 5 and 6, as no hotspots are observed in these data sets. For all three dots, we find negligible saturation constants $T_{1,\mathrm{sat}}^{-1}$. On the basis of the longest observed relaxation time for this device, we estimate $T_{1,\mathrm{sat}}^{-1} < 0.2$ Hz. Finally, at high fields we observe a variety of power-law exponents, with $p = 5.5$, 4.0, and 4.7 for dots 2, 5, and 6, respectively.

While the data are well fit by Eq. (1), it contains empirical fit parameters. We therefore seek to constrain our fits by turning to existing theoretical models. Relaxation is expected to be dominated by spin-orbit and spin-valley coupling, both of which have been considered in detail for Si quantum dots and can be distinguished by their characteristic magnetic field dependence [36,37,43]. Spin-orbit coupling leads to spin relaxation through coupling to higher orbital states and is described by the functional form

$$T_{1,SO}^{-1} \propto \frac{\omega_Z^2}{\omega_d^4} S(\omega_Z), \tag{3}$$

where ω_d is the orbital confinement frequency and $S(\omega_Z)$ is the electrical noise spectrum at frequency ω_Z [2,37]. The spin-valley contribution is described by

$$T_{1,SV}^{-1}(\omega_Z) \propto S(\omega_Z) F_{SV}(\omega_Z), \tag{4}$$

with F_{SV} as previously defined. Both rates are dependent on the noise spectrum $S(\omega_Z)$, which can have contributions from Johnson noise, charge noise, and phonons [37]. Johnson noise, which may be caused by charge fluctuations in the resistive leads of the quantum dots, results in a noise spectrum $S_J(\omega_Z) \propto \omega_Z \coth(\hbar\omega_Z/2k_BT_e)$, where T_e is the electron temperature [37,44]. Charge noise, often related to the occupation and ionization of nearby charge traps [45–47], yields $S_{\mathrm{ch}}(\omega_Z) \propto T_e/\omega_Z$. Phonons, which can couple to the electron through electric fields generated by crystal-lattice deformations [15,36,37], have a strong energy dependence, $S_{\mathrm{ph}}(\omega_Z) \propto \omega_Z^5 \coth(\hbar\omega_Z/2k_BT_{\mathrm{lat}})$.

In the low-temperature limit ($k_BT_e \ll \hbar\omega_Z$) valid in our measurements, $\coth(\hbar\omega_Z/2k_BT_e) \approx 1$ and the spin-valley relaxation contributions mediated by Johnson noise and phonons explain the relaxation hotspots in the data. However, it is not possible to clearly identify the combination of existing spin-orbit and spin-valley relaxation theories with the noise terms considered to account for the low-field saturation of T_1 in device 1 and the high-field scaling of T_1 in both devices.

To obtain further insight into the mechanisms that lead to the behavior at low and high fields, we take two additional data sets. We first examine the low-field saturation of T_1 in the right dot of device 1. We begin by measuring the resonance frequency of the electron spin in the right quantum dot at external fields $B_{\mathrm{ext}} = 250$ (500) mT, resulting in $f_R = 10.2$ (17.9) GHz, corresponding to $B_{\mathrm{tot}} = 360$ (640) mT. This confirms that the external field continues to dominate at low fields, indicating that the low-field behavior is of physical origin and not an artifact due to the magnetic field contribution from B_m. The observed saturation could conceivably be due to charge-noise-induced motion in a large transverse magnetic field gradient. We therefore set $B_{\mathrm{ext}} = 250$ mT and measure T_1 as a function of the white-noise power S_{rf} applied to gate R, coupling to the right-dot chemical potential. This artificial charge noise is generated by an arbitrary waveform generator and is up-converted to the resonance frequency of the electron spin $f_R = 10.2$ GHz with use of the mixing input of a vector signal generator. We calibrate the applied power by measuring the Rabi frequency of the right spin as a function of applied microwave power when using a coherent drive. We then make comparisons with finite-element electromagnetic field simulations to extract the ac electric field amplitude at the right spin. Knowing the power of the noise generated by the source, we can then estimate the noise spectral density at the device [41]. As shown in Fig. 4(a), T_1^{-1} increases linearly with S_{rf}.

Since the spin relaxation rate is proportional to the noise power spectral density, we can extract an estimate for the magnitude of the internal noise S_{int} in the device that leads to the low-power saturation of T_1. Specifically, since the internal noise and the artificial noise are uncorrelated, their noise power spectral densities add linearly and we expect the relaxation rate to double when $S_{\mathrm{rf}} = S_{\mathrm{int}}$. By meeting this condition at $T_1^{-1} = 12$ Hz and $S_{\mathrm{rf}} = -187$ dBm/Hz, we infer the internal noise. This power translates to a voltage noise $S_V(f_R) = 0.2$ $\mathrm{nV_{rms}}/\sqrt{\mathrm{Hz}}$ at the gate if we assume there is a high impedance load [41]. Applying $1/f$ scaling of the noise source, and factoring in the lever-arm conversion between gate voltage and energy $\alpha = 0.13$ e, we find that this noise level corresponds to $S_V \approx 20$ $\mu\mathrm{V}/\sqrt{\mathrm{Hz}} \approx 3$ $\mu\mathrm{eV}/\sqrt{\mathrm{Hz}}$ at 1 Hz, which is consistent with charge-noise values reported in the literature [48,49]. Together with the observed variation of saturation between the two dots and the generally enhanced relaxation compared with device 2, this indicates that in the presence of a magnetic field gradient, T_1 sensitively depends on the local noise environment, the strength of the transverse field gradient, and the valley splitting.

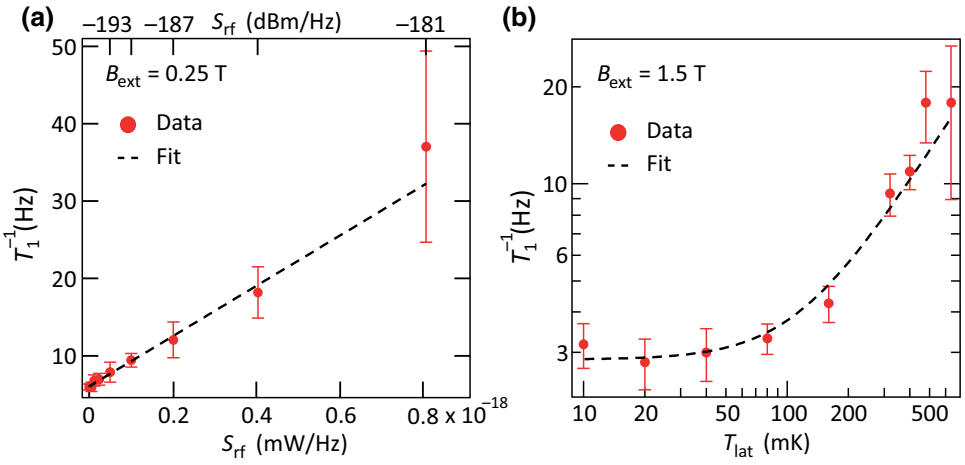

FIG. 4. Effects of noise and temperature on T_1. (a) In the low-field regime ($B_{ext} = 0.25$ T) on device 1, where T_1 saturates, we drive gate R with white noise with power spectral density S_{rf}. We find $T_1^{-1} \propto S_{rf}$ (dashed line). (b) With $B_{ext} = 1.5$ T on device 2, we measure $T_1(T_{lat})$. Taking into account the minimum electron temperature, $T_0 = 115$ mK, we find that $T_1^{-1} \propto T_e = \sqrt{T_0^2 + T_{lat}^2}$.

Next we investigate the mechanism leading to the high-field behavior of T_1 in both devices. On the basis of theoretical models for first-order relaxation processes considered, the low-temperature limit still holds up to $T \approx 1$ K at $B_{ext} > 1$ T, implying a temperature independence of T_1. However, higher-order processes might show a temperature dependence at lower T [33,50]. To reduce the impact of the known spin-valley contribution, we perform this measurement in dot 6 of device 2 where no hotspot is observed. We fix the magnetic field at $B_{ext} = 1.5$ T and measure T_1 as a function of the lattice temperature T_{lat}, which is controlled by heating the mixing chamber plate of the dilution refrigerator. We fit the data shown in Fig. 4(b) to the form

$$T_1^{-1}(T_{lat}) = c\sqrt{T_0^2 + T_{lat}^2}, \tag{5}$$

where $T_0 = 115$ mK is the base electron temperature in device 2, c is an overall scaling factor, and $\sqrt{T_0^2 + T_{lat}^2} \equiv T_e$ is the effective electron temperature. We find that the relaxation rate increases linearly with T_e, even though we expect no temperature dependence. While more studies are needed, this suggests that the high-field behavior is not adequately described by the first-order processes considered. Together with the observed variation of power laws and the absence of relaxation hotspots in the data from device 2, low-lying excited valley states may be accessed in higher-order relaxation processes.

IV. CONCLUSION

In conclusion, we measure the spin relaxation time T_1 as a function of magnetic field in Si/SiGe quantum dots. A micromagnet accelerates spin relaxation over the entire range of magnetic fields and results in saturation of the relaxation time at low magnetic fields. A smaller T_1 will adversely impact the read-out visibility in large quantum-dot arrays, where the measurement time can be a significant fraction of T_1 [39]. Our results imply that careful engineering of the micromagnet will be crucial for improving the performance of quantum-dot devices incorporating micromagnets. This will manifest itself in a trade-off between control speed and spin relaxation by finding a compromise in gradient field strength, but also the development of dynamic control of the field gradient, through either spatial or temporal modulation, allowing *in situ* control over the synthetic spin-orbit field strength. Of course, careful engineering will require a full theoretical understanding of the microscopic mechanisms responsible for spin relaxation in the presence of large magnetic field gradients.

ACKNOWLEDGMENTS

We thank X. Hu and P. Huang for helpful discussions. This research was sponsored by the Army Research Office through Grant No. W911NF-15-1-0149, the Gordon and Betty Moore Foundation's EPiQS Initiative through Grant No. GBMF4535, and the NSF through Grant No. DMR-1409556. The devices were fabricated in the Princeton University Quantum Device Nanofabrication Laboratory.

[1] D. Loss and D. P. DiVincenzo, Quantum computation with quantum dots, Phys. Rev. A **57**, 120 (1998).
[2] R. Hanson, L. P. Kouwenhoven, J. R. Petta, S. Tarucha, and L. M. K. Vandersypen, Spins in few-electron quantum dots, Rev. Mod. Phys. **79**, 1217 (2007).
[3] F. H. L. Koppens, C. Buizert, K. J. Tielrooij, I. T. Vink, K. C. Nowack, T. Meunier, L. P. Kouwenhoven, and L. M. K. Vandersypen, Driven coherent oscillations of a single electron spin in a quantum dot, Nature (London) **442**, 766 (2006).
[4] M. Veldhorst, J. C. C. Hwang, C. H. Yang, A. W. Leenstra, B. de Ronde, J. P. Dehollain, J. T. Muhonen, F. E. Hudson, K. M. Itoh, A. Morello, and A. S. Dzurak, An addressable quantum dot qubit with fault-tolerant control-fidelity, Nat. Nanotechnol. **9**, 981 (2014).

[5] K. C. Nowack, F. H. L. Koppens, Y. V. Nazarov, and L. M. K. Vandersypen, Coherent control of a single electron spin with electric fields, Science **318**, 1430 (2007).
[6] S. Nadj-Perge, S. M. Frolov, E. P. A. M. Bakkers, and L. P. Kouwenhoven, Spin–orbit qubit in a semiconductor nanowire, Nature (London) **468**, 1084 (2010).
[7] K. D. Petersson, L. W. McFaul, M. D. Schroer, M. Jung, J. M. Taylor, A. A. Houck, and J. R. Petta, Circuit quantum electrodynamics with a spin qubit, Nature (London) **490**, 380 (2012).
[8] M. Pioro-Ladrière, T. Obata, Y. Tokura, Y.-S. Shin, T. Kubo, K. Yoshida, T. Taniyama, and S. Tarucha, Electrically driven single-electron spin resonance in a slanting Zeeman field, Nat. Phys. **4**, 776 (2008).
[9] J. Yoneda, K. Takeda, T. Otsuka, T. Nakajima, M. R. Delbecq, G. Allison, T. Honda, T. Kodera, S. Oda, Y. Hoshi, N. Usami, K. M. Itoh, and S. Tarucha, A quantum-dot spin qubit with coherence limited by charge noise and fidelity higher than 99.9%, Nat. Nanotechnol. **13**, 102 (2018).
[10] J. R. Petta, A. C. Johnson, J. M. Taylor, E. A. Laird, A. Yacoby, M. D. Lukin, C. M. Marcus, M. P. Hanson, and A. C. Gossard, Coherent manipulation of coupled electron spins in semiconductor quantum dots, Science **309**, 2180 (2005).
[11] M. Veldhorst, C. H. Yang, J. C. C. Hwang, W. Huang, J. P. Dehollain, J. T. Muhonen, S. Simmons, A. Laucht, F. E. Hudson, K. M. Itoh, A. Morello, and A. S. Dzurak, A two-qubit logic gate in silicon, Nature (London) **526**, 410 (2015).
[12] D. M. Zajac, A. J. Sigillito, M. Russ, F. Borjans, J. M. Taylor, G. Burkard, and J. R. Petta, Resonantly driven CNOT gate for electron spins, Science **359**, 439 (2018).
[13] T. F. Watson, S. G. J. Philips, E. Kawakami, D. R. Ward, P. Scarlino, M. Veldhorst, D. E. Savage, M. G. Lagally, M. Friesen, S. N. Coppersmith, M. A. Eriksson, and L. M. K. Vandersypen, A programmable two-qubit quantum processor in silicon, Nature (London) **555**, 633 (2018).
[14] A. Morello, J. J. Pla, F. A. Zwanenburg, K. W. Chan, K. Y. Tan, H. Huebl, M. Möttönen, C. D. Nugroho, C. Yang, J. A. van Donkelaar, A. D. C. Alves, D. N. Jamieson, C. C. Escott, L. C. L. Hollenberg, R. G. Clark, and A. S. Dzurak, Single-shot readout of an electron spin in silicon, Nature (London) **467**, 687 (2010).
[15] C. H. Yang, A. Rossi, R. Ruskov, N. S. Lai, F. A. Mohiyaddin, S. Lee, C. Tahan, G. Klimeck, A. Morello, and A. S. Dzurak, Spin-valley lifetimes in a silicon quantum dot with tunable valley splitting, Nat. Commun. **4**, 2069 (2013).
[16] J. J. Pla, K. Y. Tan, J. P. Dehollain, W. H. Lim, J. J. L. Morton, D. N. Jamieson, A. S. Dzurak, and A. Morello, A single-atom electron spin qubit in silicon, Nature (London) **489**, 541 (2012).
[17] L. V. C. Assali, H. M. Petrilli, R. B. Capaz, B. Koiller, X. Hu, and S. Das Sarma, Hyperfine interactions in silicon quantum dots, Phys. Rev. B **83**, 165301 (2011).
[18] J. T. Muhonen, J. P. Dehollain, A. Laucht, F. E. Hudson, R. Kalra, T. Sekiguchi, K. M. Itoh, D. N. Jamieson, J. C. McCallum, A. S. Dzurak, and A. Morello, Storing quantum information for 30 seconds in a nanoelectronic device, Nat. Nanotechnol. **9**, 986 (2014).
[19] A. M. Tyryshkin, S. Tojo, J. J. L. Morton, H. Riemann, N. V. Abrosimov, P. Becker, H.-J. Pohl, T. Schenkel, M. L. W. Thewalt, K. M. Itoh, and S. A. Lyon, Electron spin coherence exceeding seconds in high-purity silicon, Nat. Mater. **11**, 143 (2012).
[20] M. Steger, K. Saeedi, M. L. W. Thewalt, J. J. L. Morton, H. Riemann, N. V. Abrosimov, P. Becker, and H.-J. Pohl, Quantum information storage for over 180 s using donor spins in a ^{28}Si "semiconductor vacuum", Science **336**, 1280 (2012).
[21] A. V. Khaetskii and Y. V. Nazarov, Spin-flip transitions between Zeeman sublevels in semiconductor quantum dots, Phys. Rev. B **64**, 125316 (2001).
[22] V. I. Fal'ko, B. L. Altshuler, and O. Tsyplyatyev, Anisotropy of Spin Splitting and Spin Relaxation in Lateral Quantum Dots, Phys. Rev. Lett. **95**, 076603 (2005).
[23] A. V. Khaetskii, D. Loss, and L. Glazman, Electron Spin Decoherence in Quantum Dots due to Interaction with Nuclei, Phys. Rev. Lett. **88**, 186802 (2002).
[24] V. N. Golovach, A. Khaetskii, and D. Loss, Phonon-Induced Decay of the Electron Spin in Quantum Dots, Phys. Rev. Lett. **93**, 016601 (2004).
[25] T. Meunier, I. T. Vink, L. H. W. van Beveren, K.-J. Tielrooij, R. Hanson, F. H. L. Koppens, H. P. Tranitz, W. Wegscheider, L. P. Kouwenhoven, and L. M. K. Vandersypen, Experimental Signature of Phonon-Mediated Spin Relaxation in a Two-Electron Quantum Dot, Phys. Rev. Lett. **98**, 126601 (2007).
[26] A. C. Johnson, J. R. Petta, J. M. Taylor, A. Yacoby, M. D. Lukin, C. M. Marcus, M. P. Hanson, and A. C. Gossard, Triplet–singlet spin relaxation via nuclei in a double quantum dot, Nature (London) **435**, 925 (2005).
[27] P. Scarlino, E. Kawakami, P. Stano, M. Shafiei, C. Reichl, W. Wegscheider, and L. Vandersypen, Spin-Relaxation Anisotropy in a GaAs Quantum Dot, Phys. Rev. Lett. **113**, 256802 (2014).
[28] S. Amasha, K. MacLean, I. P. Radu, D. M. Zumbühl, M. A. Kastner, M. P. Hanson, and A. C. Gossard, Electrical Control of Spin Relaxation in a Quantum Dot, Phys. Rev. Lett. **100**, 046803 (2008).
[29] M. Kroutvar, Y. Ducommun, D. Heiss, M. Bichler, D. Schuh, G. Abstreiter, and J. J. Finley, Optically programmable electron spin memory using semiconductor quantum dots, Nature **432**, 81 (2004).
[30] L. C. Camenzind, L. Yu, P. Stano, J. D. Zimmerman, A. C. Gossard, D. Loss, and D. M. Zumbuhl, Hyperfine-phonon spin relaxation in a single-electron GaAs quantum dot, Nature Commun. **9**, 3454 (2018).
[31] D. M. Zajac, T. M. Hazard, X. Mi, K. Wang, and J. R. Petta, A reconfigurable gate architecture for Si/SiGe quantum dots, Appl. Phys. Lett. **106**, 223507 (2015).
[32] M. Xiao, M. G. House, and H. W. Jiang, Measurement of the Spin Relaxation Time of Single Electrons in a Silicon Metal-Oxide-Semiconductor-Based Quantum Dot, Phys. Rev. Lett. **104**, 096801 (2010).
[33] L. Petit, J. M. Boter, H. G. J. Eenink, G. Droulers, M. L. V. Tagliaferri, R. Li, D. P. Franke, K. J. Singh, J. S. Clarke, R. N. Schouten, V. V. Dobrovitski, L. M. K. Vandersypen, and M. Veldhorst, Spin Lifetime and Charge Noise in Hot

Silicon Quantum Dot Qubits, Phys. Rev. Lett. **121**, 076801 (2018).

[34] R. R. Hayes, A. A. Kiselev, M. G. Borselli, S. S. Bui, E. T. Croke III, P. W. Deelman, B. M. Maune, I. Milosavljevic, J.-S. Moon, R. S. Ross, A. E. Schmitz, M. F. Gyure, and A. T. Hunter, arXiv:0908.0173.

[35] C. B. Simmons, J. R. Prance, B. J. Van Bael, T. S. Koh, Z. Shi, D. E. Savage, M. G. Lagally, R. Joynt, M. Friesen, S. N. Coppersmith, and M. A. Eriksson, Tunable Spin Loading and T_1 of a Silicon Spin Qubit Measured by Single-Shot Readout, Phys. Rev. Lett. **106**, 156804 (2011).

[36] C. Tahan and R. Joynt, Relaxation of excited spin, orbital, and valley qubit states in ideal silicon quantum dots, Phys. Rev. B **89**, 075302 (2014).

[37] P. Huang and X. Hu, Spin relaxation in a Si quantum dot due to spin-valley mixing, Phys. Rev. B **90**, 235315 (2014).

[38] X. Mi, T. M. Hazard, C. Payette, K. Wang, D. M. Zajac, J. V. Cady, and J. R. Petta, Magnetotransport studies of mobility limiting mechanisms in undoped Si/SiGe heterostructures, Phys. Rev. B **92**, 035304 (2015).

[39] D. M. Zajac, T. M. Hazard, X. Mi, E. Nielsen, and J. R. Petta, Scalable Gate Architecture for a One-Dimensional Array of Semiconductor Spin Qubits, Phys. Rev. Appl. **6**, 054013 (2016).

[40] J. M. Elzerman, R. Hanson, L. H. Willems van Beveren, B. Witkamp, L. M. K. Vandersypen, and L. P. Kouwenhoven, Single-shot read-out of an individual electron spin in a quantum dot, Nature (London) **430**, 431 (2004).

[41] See Supplemental Material at http://link.aps.org/supplemental/10.1103/PhysRevApplied.11.044063 for additional data and measurement details, and which includes Refs. [8,35,39,51,52].

[42] X. Mi, C. G. Peterfalvi, G. Burkard, and J. R. Petta, High-Resolution Valley Spectroscopy of Si Quantum Dots, Phys. Rev. Lett. **119**, 176803 (2017).

[43] C. Tahan, Silicon in the Quantum Limit: Quantum Computing and Decoherence in Silicon Architectures, arXiv:0710.4263 [cond-mat].

[44] U. Weiss, *Quantum Dissipative Systems* (World Scientific, Singapore, 1999).

[45] E. Paladino, Y. Galperin, G. Falci, and B. Altshuler, $1/f$ noise: Implications for solid-state quantum information, Rev. Mod. Phys. **86**, 361 (2014).

[46] A. Bermeister, D. Keith, and D. Culcer, Charge noise, spin-orbit coupling, and dephasing of single-spin qubits, Appl. Phys. Lett. **105**, 192102 (2014).

[47] P. Huang and X. Hu, Electron spin relaxation due to charge noise, Phys. Rev. B **89**, 195302 (2014).

[48] B. M. Freeman, J. S. Schoenfield, and H. Jiang, Comparison of low frequency charge noise in identically patterned Si/SiO_2 and Si/SiGe quantum dots, Appl. Phys. Lett. **108**, 253108 (2016).

[49] K. D. Petersson, J. R. Petta, H. Lu, and A. C. Gossard, Quantum Coherence in a One-Electron Semiconductor Charge Qubit, Phys. Rev. Lett. **105**, 246804 (2010).

[50] K. N. Shrivastava, Theory of spin–lattice relaxation, Phys. Status Solidi (b) **117**, 437 (1983).

[51] Y. Tokura, W. G. van der Wiel, T. Obata, and S. Tarucha, Coherent Single Electron Spin Control in a Slanting Zeeman Field, Phys. Rev. Lett. **96**, 047202 (2006).

[52] E. Kawakami, P. Scarlino, D. R. Ward, F. R. Braakman, D. E. Savage, M. G. Lagally, M. Friesen, S. N. Coppersmith, M. A. Eriksson, and L. M. K. Vandersypen, Electrical control of a long-lived spin qubit in a Si/SiGe quantum dot, Nat. Nanotechnol. **9**, 666 (2014).